Robust and Data-efficient Q-learning by Composite Value-estimation

Anonymous authors
Paper under double-blind review

Abstract

In the past few years, off-policy reinforcement learning methods have shown promising results in their application for robot control. Deep Q-learning, however, still suffers from poor data-efficiency and is susceptible to stochasticity or noise in transitions and reward, which is limiting with regard to real-world applications. We alleviate these problems by proposing two novel off-policy Temporal-Difference formulations: (1) Truncated Q-functions which represent the return for the first n steps of a target-policy rollout w.r.t. the full action-value and (2) Shifted Q-functions, acting as the farsighted return after this truncated rollout. This decomposition allows us to optimize both parts with their individual learning rates, achieving significant learning speedup and robustness to variance in the reward signal, leading to the Composite Q-learning algorithm. We employ Composite Q-learning within TD3 and compare Composite TD3 with TD3 and TD3(Δ), which we introduce as an off-policy variant of TD(Δ). Moreover, we show that Composite TD3 outperforms TD3 as well as TD3(Δ) significantly in terms of data-efficiency in multiple simulated robot tasks and that Composite Q-learning is robust to stochastic environments and reward functions.

1 Introduction

In recent years, Q-learning (Watkins & Dayan, 1992) has achieved major successes in a broad range of areas by employing deep neural networks (Mnih et al., 2015; Silver et al., 2018; Lillicrap et al., 2016), including environments of higher complexity (Riedmiller et al., 2018) and even in first real-world applications (Haarnoja et al., 2019). Deep Q-learning methods, however, are still far away from being easily applicable to solving complex real-world robotic tasks due to their high demand for data samples and their lack in learning stability caused by the stochastic nature of transitions in real-world settings. Especially stochasticity in the immediate reward signal itself may cause policies to converge to suboptimal performance. This stochasticity can be induced by multiple sources of randomness, e.g. through stochastic next state transitions due to sensor or actuator noise, occlusions, or due to data-driven reward estimation (Authors, 2020a; Ni et al., 2020; Fu et al., 2018). This increases the complexity of value-estimation tremendously due the long temporal horizon the reward signal has to propagate through, possibly depending on many decision steps and transitions. To overcome the complexity of growing task horizon, in this work, we propose to break down the long-term return into a composition of several short-term predictions over a *fixed temporal horizon*. We approach this via a new formulation of consecutive bootstrapping from value-functions corresponding to different horizons of the target-policy associated to the *full return*. For its formulation, we define *Truncated Q-functions*, representing the return for the first n steps of a target-policy rollout w.r.t. the full action-value. In addition, we introduce *Shifted Q-functions* which represent the farsighted return after this truncated rollout. Both are then combined in a mutual recursive definition of the Q-function for the final algorithm. Starting from a reformulation of the vanilla Q-learning formalism, our approach offers the flexibility to separately optimize hyperparameters for different parts of value-estimation, showing that Shifted Q-functions suffer less from variance compared to the full return thus allowing for higher learning rates.

Most similar to our approach is TD(Δ) (Romoff et al., 2019), composing the full return of value-functions with increasing discount. Increasing discount factors translate to growing task horizons, leading to a decomposition of the long-term prediction task into multiple subtasks of smaller complexity. In their work, Romoff

et al. (2019) argue that values for smaller discount values can potentially stabilize more quickly, leading to faster and more stable learning. Since the values corresponding to larger discount values only represent the residual to the values of smaller discount, however, TD(Δ) does not alleviate the issues arising in stochastic environments. Other techniques for variance reduction in TD-learning are reward estimation (Romoff et al., 2018) or averaging value-functions (Anschel et al., 2017). Both techniques are orthogonal to our work and can be combined with Composite Q-learning to possibly further enhance learning stability. However, as we show in this work, the increase in performance and data-efficiency comes from the possibility of higher learning rates in the long-term Shifted Q-functions and not the short-sighted Truncated Q-functions. It can thus be argued that reward estimation and averaging come at a cost of slower convergence. Asis et al. (2020) propose to learn action-values for a fixed-horizon via consecutive bootstrapping. In their formulation, however, the consecutive value-functions are estimated over different target-policies w.r.t. the different horizons and ignore the residual of the full return. Thus, they can therefore be non-optimal w.r.t. the task at hand.

Our contributions are fourfold. First, we introduce the *Composite Q-learning* algorithm. Second, we show that the targets of Shifted Q-functions suffer less from variance compared to the full action-value, thus allowing for higher learning rates. Third, we introduce *TD3*(Δ), an off-policy extension of TD(Δ) to deep Q-learning. And fourth, we employ Composite Q-learning within TD3 and evaluate Composite TD3 in various simulated robot tasks under normal and noisy reward functions.

2 Background

We consider tasks modelled as Markov decision processes (MDP), where an agent executes action $a_t \in \mathcal{A}$ in some state $s_t \in \mathcal{S}$ following its stochastic policy $\pi : \mathcal{S} \times \mathcal{A} \mapsto [0, 1]$. According to the dynamics model $\mathcal{M} : \mathcal{S} \times \mathcal{A} \times \mathcal{S} \mapsto [0, 1]$ of the environment, the agent transitions into some state $s_{t+1} \in \mathcal{S}$ and receives scalar reward r_t. The agent aims at maximizing the expected long-term return $\mathcal{R}^\pi(s_t) = \mathbf{E}_{a_{j\geq t}\sim\pi, s_{j>t}\sim\mathcal{M}}[\sum_{j=t}^{T-1} \gamma^{j-t} r_j | s_t]$, where T is the (possibly infinite) temporal horizon of the MDP and $\gamma \in [0, 1]$ the discount factor. It therefore tries to find π^*, s.t. $\mathcal{R}^{\pi^*} \geq \mathcal{R}^\pi$ for all π. If the model of the environment is unknown, model-free methods based on the Bellman Optimality Equation over the so-called action-value $Q^\pi(s_t, a_t) = \mathbf{E}_{a_{j>t}\sim\pi, s_{j>t}\sim\mathcal{M}}[\sum_{j=t}^{T-1} \gamma^{j-t} r_j | s_t, a_t]$, can be used:

$$Q^*(s_t, a_t) = r_t + \gamma \max_a \mathbf{E}_{s_{j>t}\sim\mathcal{M}} \left[Q^*(s_{t+1}, a) \right]. \tag{1}$$

In the following, we abbreviate $\mathbf{E}_{a_{j>t}\sim\pi, s_{j>t}\sim\mathcal{M}}[\cdot|s_t, a_t]$ by $\mathbf{E}_{\pi,\mathcal{M}}[\cdot]$. One of the most popular model-free reinforcement learning methods is the sampling-based off-policy *Q-learning* algorithm (Watkins & Dayan, 1992). A representative of continuous model-free reinforcement learning with function approximation is the *Deep Deterministic Policy Gradient* (DDPG) actor-critic method (Lillicrap et al., 2016). In DDPG, actor μ is a deterministic mapping from states to actions, $\mu : \mathcal{S} \mapsto \mathcal{A}$, representing the actions that maximize the critic Q, i.e. $\mu(s_t) = \arg\max_a Q(s_t, a)$. Q and μ are estimated by function approximators $Q(\cdot, \cdot|\theta^Q)$ and $\mu(\cdot|\theta^\mu)$, parameterized by θ^Q and θ^μ. The critic is optimized on the mean squared error between predictions $Q(s_j, a_j|\theta^Q)$ and targets $y_j = r_j + \gamma Q'(s_{j+1}, \mu'(s_{j+1}|\theta^{\mu\prime})|\theta^{Q\prime})$, where Q' and μ' are target networks, parameterized by $\theta^{Q\prime}$ and $\theta^{\mu\prime}$. The parameters of μ are optimized following the deterministic policy gradient theorem (Silver et al., 2014), $\nabla_{\theta^\mu} \hookleftarrow \frac{1}{m} \sum_j \nabla_a Q(s, a|\theta^Q)|_{s=s_j, a=\mu(s_j|\theta^\mu)} \nabla_{\theta^\mu} \mu(s|\theta^\mu)$, and the parameters of the target networks are updated via Polyak averaging, i.e. $\theta^{Q\prime} \hookleftarrow (1-\tau)\theta^{Q\prime} + \tau\theta^Q$ and $\theta^{\mu\prime} \hookleftarrow (1-\tau)\theta^{\mu\prime} + \tau\theta^\mu$, with $\tau \in [0, 1]$.

The state-of-the-art actor-critic method TD3 (Fujimoto et al., 2018) then adds three adjustments to vanilla DDPG. First, the minimum prediction of two distinct critics is taken for target calculation to alleviate overestimation bias, an approach belonging to the family of Double Q-learning algorithms (van Hasselt et al., 2016). Second, Gaussian smoothing is applied to the target-policy, addressing the variance in updates. Third, actor and target networks are updated every d-th gradient step of the critic, to account for the problem of moving targets.

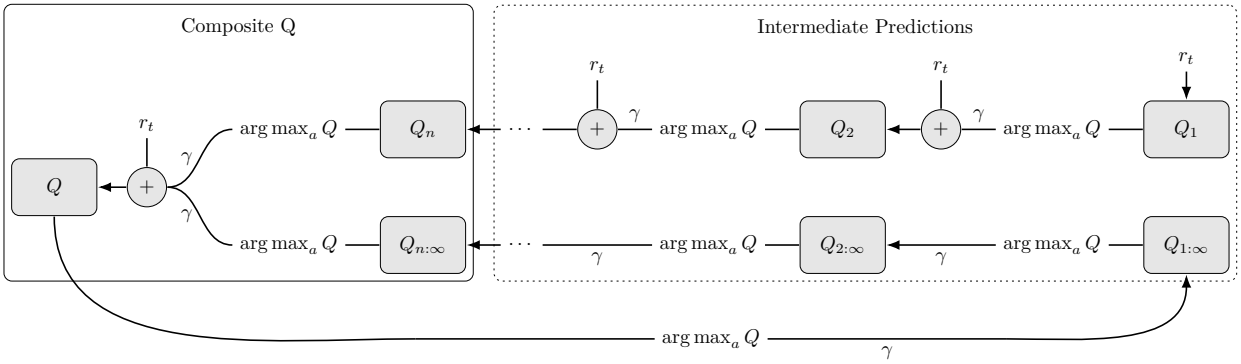

Figure 1: Structure of Composite Q-learning. Q_i denote the Truncated and $Q_{i:\infty}$ the Shifted Q-functions at step i. Q is the complete Composite Q-function. Directed incoming edges yield the targets for the corresponding value-function, evaluated at the maximizing actions of the full Q-function. Edges denoted by γ are discounted.

3 Combining Long-term and Short-term Predictions in Q-learning

In the following, we introduce the Composite Q-learning algorithm, along with Off-policy TD(Δ) as an additional baseline. Both approaches aim at decomposing the long-term value into values of smaller time scales. Composite Q-learning approaches this by dividing the bootstrapping into a short-term and a long-term component. Off-policy TD(Δ) on the other hand formalizes a delta function to estimate the remainder of an action-value corresponding to a smaller discount factor.

3.1 Composite Q-learning

We estimate the return of n-step rollouts of the target-policy via Truncated Q-functions which we then combine to the full return with model-free Shifted Q-functions, an approach we call *Composite Q-learning*, while remaining *purely off-policy*. Since these quantities cannot be estimated directly from single-step transitions, we introduce a consecutive bootstrapping scheme based on intermediate predictions. For an overview, see Figure 1. Code based on the implementation of TD3[1] can be found in the supplementary.

3.1.1 Truncated Q-functions

In order to decompose the action-value into multiple truncated returns, assume that $n \ll (T-1)$ and that $(T-1-t) \mod n = 0$ for task horizon T. We make use of the following observation:

$$\begin{aligned} Q^\pi(s_t, a_t) &= \mathbf{E}_{\pi,\mathcal{M}}\left[r_t + \gamma r_{t+1} + \gamma^2 r_{t+2} + \gamma^3 r_{t+3} + \cdots + \gamma^{T-1} r_{T-1}\right] \\ &= \mathbf{E}_{\pi,\mathcal{M}}\left[\left(\sum_{j=t}^{t+n-1} \gamma^{j-t} r_j\right) + \gamma^n \left(\sum_{j=t+n}^{t+2n-1} \gamma^{j-(t+n)} r_j\right)\right. \\ &\qquad \left. + \cdots + \gamma^{T-n}\left(\sum_{j=T-n}^{T-1} \gamma^{j-(T-n)} r_j\right)\right]. \end{aligned} \tag{2}$$

That is, we can define the action-value as a combination of partial sums of length n. We can then define the Truncated Q-function as $Q^\pi_n(s_t, a_t) = \mathbf{E}_{\pi,\mathcal{M}}[\sum_{j=t}^{t+n-1} \gamma^{j-t} r_j]$, which we plug into Equation (2):

$$Q^\pi(s_t, a_t) = \mathbf{E}_{\pi,\mathcal{M}}[Q^\pi_n(s_t, a_t) + \gamma^n Q^\pi_n(s_{t+n}, a_{t+n}) + \cdots + \gamma^{T-n} Q^\pi_n(s_{T-n}, a_{T-n})]. \tag{3}$$

Please note that the assumption of $(T-1-t) \mod n = 0$ only leads to an easier notation and is not a general restriction. If $(T-1-t) \mod n \neq 0$, then the last partial sum simply has a shorter horizon. Following

[1] https://github.com/sfujim/TD3

Theorem A.1 in the appendix, we approximate $Q^*_n(s_t, a_t)$ off-policy via consecutive bootstrapping. In order to limit the prediction to horizon n, we estimate n different truncated value-functions belonging to increasing horizons. Let $Q^{\mathrm{Tr}}(\cdot,\cdot|\theta^{\mathrm{Tr}})$ denote a function approximator with parameters θ^{Tr} and n outputs, subsequently called *heads*, estimating Truncated Q-functions Q^*_i. Each output Q^{Tr}_i bootstraps from the prediction of the preceding head evaluating the target-policy of *full* return Q for a fixed horizon, with the first approximating the immediate reward function. The targets are therefore given by:

$$\begin{aligned} y^{\mathrm{Tr}}_{j,1} &= r_j \text{ and} \\ y^{\mathrm{Tr}}_{j,i>1} &= r_j + \gamma Q^{\mathrm{Tr}\prime}_{i-1}(s_{j+1}, \mu'(s_{j+1}|\theta^{\mu\prime})|\theta^{\mathrm{Tr}\prime}), \end{aligned} \tag{4}$$

where μ' corresponds to the target-actor maximizing the full Q-value as defined in Section 2 and $Q^{\mathrm{Tr}\prime}_{i-1}$ the output of the respective Q-target-network. That is, Q^{Tr} represents evaluations of μ at different stages of truncation and $y^{\mathrm{Tr}}_{j,i<n}$ serve as intermediate predictions to get $y^{\mathrm{Tr}}_{j,n}$. We then *only* use Q^{Tr}_n, which implements the full n-step return, as the first part of the composition of the Q-target, but not the $Q^{\mathrm{Tr}}_{i<n}$ values.

Please note that in order to estimate Equation (3), the dynamics model would be needed to get $s_{t+c\cdot n}$ of a rollout starting in s_t. In the following, we describe an approach to achieve an estimation of Equation (3) model-free.

3.1.2 Shifted Q-functions

To get an estimation for the remainder of the rollout $Q^\pi_{n:\infty} = \mathbf{E}_{\pi,\mathcal{M}}[\gamma^n Q(s_{t+n}, a_{t+n})]$ after n steps, we use a consecutive bootstrapping formulation of the Q-prediction as a means to skip the first n rewards of a target-policy rollout. Let $Q^{\mathrm{Sh}}(\cdot,\cdot|\theta^{\mathrm{Sh}})$ denote the function approximator estimating the Shifted Q-functions $Q^*_{i:\infty}$ by n different outputs, parameterized by θ^{Sh}. We can shift the Q-prediction by bootstrapping without taking the immediate reward into account. The Shifted Q-targets for heads Q^{Sh}_i therefore become:

$$\begin{aligned} y^{\mathrm{Sh}}_{j,1} &= \gamma Q'(s_{j+1}, \mu'(s_{j+1}|\theta^{\mu\prime})|\theta^{Q\prime}) \text{ and} \\ y^{\mathrm{Sh}}_{j,i>1} &= \gamma Q^{\mathrm{Sh}\prime}_{i-1}(s_{j+1}, \mu'(s_{j+1}|\theta^{\mu\prime})|\theta^{\mathrm{Sh}\prime}). \end{aligned} \tag{5}$$

The variance of the remainder of the rollout decreases with later initial point in time:

$$\begin{aligned} \mathrm{var}[\gamma^i Q^\pi(s_{t+i}, a_{t+i})] &= \mathrm{var}[\gamma^i(r_{t+i} + \gamma Q^\pi(s_{t+i+1}, a_{t+i+1}))] \\ &= \mathrm{var}[\gamma^i r_{t+i}] + \mathrm{var}[\gamma^{i+1} Q^\pi(s_{t+i+1}, a_{t+i+1})] \\ &\quad + 2\,\mathrm{cov}[\gamma^i r_{t+i}, \gamma^{i+1} Q^\pi(s_{t+i+1}, a_{t+i+1})]. \end{aligned} \tag{6}$$

If $\mathrm{cov}[\gamma^i r_{t+i}, \gamma^{i+1} Q^\pi(s_{t+i+1}, a_{t+i+1})] \geq 0$, it holds that:

$$\mathrm{var}[\gamma^i Q^\pi(s_{t+i}, a_{t+i})] \geq \mathrm{var}[\gamma^{i+1} Q^\pi(s_{t+i+1}, a_{t+i+1})]. \tag{7}$$

Please note that $\gamma^i Q^\pi(s_{t+i}, a_{t+i})$ corresponds to Shifted Q-functions at different stages i of shifting, with $i = 0$ for the full Q-function. It hence follows:

$$\mathrm{var}[Q^\pi(s_t, a_t)] \geq \mathrm{var}[Q^\pi_{1:\infty}(s_t, a_t)] \geq \mathrm{var}[Q^\pi_{2:\infty}(s_t, a_t)] \geq \cdots \geq \mathrm{var}[Q^\pi_{n:\infty}(s_t, a_t)]. \tag{8}$$

The covariance of reward and future return is likely to be positive if the immediate reward depends on the next state (Romoff et al., 2018). Otherwise the covariance is zero. Hence, it can be argued that this inequality is strict if the variance of the reward is larger than zero. This also holds for the case of zero variance for the immediate reward, if the immediate reward depends on a stochastic next state. We therefore argue that in these settings, as very common in real-world experiments, Shifted Q-functions allow for higher learning rates compared to the full Q-function, since this translates to lower variance in their gradients. We empirically validate this finding in our experiments in Section 4.

3.1.3 Composition

Following the definitions of Truncated and Shifted Q-functions, we can compose the full return. In the appendix, we show that the composition is a representation of the complete Q-value and provide an analysis of Tabular Composite Q-learning. In the function approximation setting, we can define the Composite Q-target as:

$$y_j^Q = r_j + \gamma(Q_n^{\mathrm{Tr}\prime}(s_{j+1}, \mu'(s_{j+1}|\theta^{\mu\prime})|\theta^{\mathrm{Tr}\prime}) + Q_n^{\mathrm{Sh}\prime}(s_{j+1}, \mu'(s_{j+1}|\theta^{\mu\prime})|\theta^{\mathrm{Sh}\prime})), \tag{9}$$

approximated by $Q(\cdot,\cdot|\theta^Q)$ with parameters θ^Q. We jointly estimate Q^{Tr}, Q^{Sh} and Q with function approximator $Q^{\mathcal{C}}(\cdot,\cdot|\theta^{\mathcal{C}})$.

The incorporation of truncated returns divides the time scale of the long-term prediction by the Shifted Q-function. We call this algorithm *Composite Q-learning*. Please note that Composite Q-learning is equivalent to Q-learning if the learning rates for Truncated, Shifted and full Q-function are set to the same values. However, a notable advantage is that Composite Q-learning offers an independent optimization for the different learning rates corresponding to different temporal horizons. A detailed description of Deep Continuous Composite Q-learning in its general form is given in Algorithm 1. For an exemplary application within TD3 (as in our experiments in the following), Gaussian policy smoothing has to be added to all targets in Line 8, as well as taking the minimum prediction of two distinct critics for each target. Furthermore, actor and target networks have to be updated with delay.

Algorithm 1: Deep Continuous Composite Q-learning

1 initialize critic $Q^{\mathcal{C}}$, actor μ and targets $Q^{\mathcal{C}\prime}$, μ'
2 initialize replay buffer $\mathcal{R}$
3 **for** *episode* $= 1..E$ **do**
4 get initial state s_1
5 **for** $t = 1..T$ **do**
6 apply action $a_t = \mu(s_t|\theta^\mu) + \xi$, where $\xi \sim \mathcal{N}(0, \sigma)$
7 observe s_{t+1} and r_t and save transition (s_t, a_t, s_{t+1}, r_t) in $\mathcal{R}$
8 calculate targets:
$y_{j,1}^{\mathrm{Tr}} = r_j$
$y_{j,i>1}^{\mathrm{Tr}} = r_j + \gamma Q_{i-1}^{\mathrm{Tr}\prime}(s_{j+1}, \mu'(s_{j+1}|\theta^{\mu\prime})|\theta^{\mathrm{Tr}\prime})$
$y_{j,1}^{\mathrm{Sh}} = \gamma Q'(s_{j+1}, \mu'(s_{j+1}|\theta^{\mu\prime})|\theta^{Q\prime})$
$y_{j,i>1}^{\mathrm{Sh}} = \gamma Q_{i-1}^{\mathrm{Sh}\prime}(s_{j+1}, \mu'(s_{j+1}|\theta^{\mu\prime})|\theta^{\mathrm{Sh}\prime})$
$y_j^Q = r_j + \gamma(Q_n^{\mathrm{Tr}\prime}(s_{j+1}, \mu'(s_{j+1}|\theta^{\mu\prime})|\theta^{\mathrm{Tr}\prime}) + Q_n^{\mathrm{Sh}\prime}(s_{j+1}, \mu'(s_{j+1}|\theta^{\mu\prime})|\theta^{\mathrm{Sh}\prime}))$
$y_j^{\mathcal{C}} = \left[y_j^Q, y_{j,1}^{\mathrm{Tr}}, y_{j,i>1}^{\mathrm{Tr}}, y_{j,1}^{\mathrm{Sh}}, y_{j,i>1}^{\mathrm{Sh}}\right]$
9 update $Q^{\mathcal{C}}$ on minibatch b of size m from $\mathcal{R}$ update μ on Q
10 adjust parameters of $Q^{\mathcal{C}\prime}$ and μ'

3.2 Off-policy TD(Δ)

Another way to divide the value-function into multiple time scales is TD(Δ) (Romoff et al., 2019). To this point, it has only been applied in an on-policy setting. In favor of comparability, we extend TD(Δ) to Q-learning, yielding TD3(Δ). The main idea of TD(Δ) is the combination of different value-functions corresponding to increasing discount values. Let γ^Δ denote a fixed ordered sequence of increasing discount values, i.e. $\gamma^\Delta = (\gamma_1, \gamma_2, \ldots, \gamma_k)^\top|_{\gamma_{i>1}>\gamma_{i-1}}$.

We can then define delta functions W_i as:

$$W_1 = Q_{\gamma_1} \text{ and } W_{i>1} = Q_{\gamma_i} - Q_{\gamma_{i-1}}. \tag{10}$$

Let $Q^\Delta(\cdot,\cdot|\theta^\Delta)$ denote the function approximator estimating $Q_{\gamma_{1\leq i\leq k}}$ with parameters θ^Δ. Based on the derivations in (Romoff et al., 2019), the targets for Q-learning can be formalized as:

$$\begin{aligned} y_{j,1}^\gamma &= r_j + \gamma_1 Q'_{\gamma_1}(s_{j+1}, \mu'(s_{j+1}|\theta^{\mu\prime})|\theta^{\Delta\prime}) \text{ and} \\ y_{j,i>1}^\gamma &= (\gamma_i - \gamma_{i-1}) Q'_{\gamma_{i-1}}(s_{j+1}, \mu'(s_{j+1}|\theta^{\mu\prime})|\theta^{\Delta\prime}) + \gamma_i W'_i(s_{j+1}, \mu'(s_{j+1}|\theta^{\mu\prime})|\theta^{\Delta\prime}). \end{aligned} \tag{11}$$

The authors suggest the use of n-step targets within TD(Δ) which is not easily applicable in an off-policy setting. In our experiments, we therefore compare our approach to single-step Off-policy TD(Δ). A detailed overview of Off-policy TD(Δ) can be found in Algorithm 2. To transform Off-policy TD(Δ) to TD3(Δ), the adjustments as described in Section 3.1.3 have to be applied analogously.

Algorithm 2: Off-policy TD(Δ)

initialize critic Q^{Δ}, actor μ and targets $Q^{\Delta\prime}$, μ'
initialize replay buffer $\mathcal{R}$
set discount values $\gamma^{\Delta} = (\gamma_0, \gamma_1, \ldots, \gamma_k)^{\intercal}$
for $episode = 1..E$ **do**
  get initial state s_1
  for $t = 1..T$ **do**
    apply action $a_t = \mu(s_t|\theta^{\mu}) + \xi$, where $\xi \sim \mathcal{N}(0, \sigma)$
    observe s_{t+1} and r_t and save transition (s_t, a_t, s_{t+1}, r_t) in $\mathcal{R}$
    calculate targets:
      $y^{\gamma}_{j,1} = r_j + \gamma_1 Q'_{\gamma_1}(s_{j+1}, \mu'(s_{j+1}|\theta^{\mu\prime})|\theta^{\Delta\prime})$
      $y^{\gamma}_{j,i>1} = (\gamma_i - \gamma_{i-1}) Q'_{\gamma_{i-1}}(s_{j+1}, \mu'(s_{j+1}|\theta^{\mu\prime})|\theta^{\Delta\prime})$
        $+\gamma_i W'_i(s_{j+1}, \mu'(s_{j+1}|\theta^{\mu\prime})|\theta^{\Delta\prime})$
    update Q^{Δ} on minibatch b of size m from $\mathcal{R}$
    update μ on Q_{γ_k}
    adjust parameters of $Q^{\Delta\prime}$ and μ'

4 Experimental Results

We apply Composite Q-learning within TD3 and compare against TD3 and TD3(Δ) on three robot simulation tasks of OpenAI Gym (Brockman et al., 2016) based on MuJoCo (Todorov et al., 2012): Walker2d-v2, Hopper-v2 and Humanoid-v2. A visualization of the environments is depicted in Figure 2. We discuss hyperparameter optimization and hyperparameter settings, as well as the optimization procedure in Appendix D. Whilst we employ Composite Q-learning within TD3, for Soft Actor-Critic (Haarnoja et al., 2018) the same results can be assumed to hold (Ball & Roberts, 2021). We analyze the properties of Composite Q-learning in terms of data-efficiency and stability on the true reward for Walker2d-v2 and the potential increase of updates per sample for Walker2d-v2 and Hopper-v2 in Section 4.1, before we evaluate Composite TD3 on a very noisy reward signal for Walker2d-v2, Hopper-v2 and Humanoid-v2 in Section 4.2.

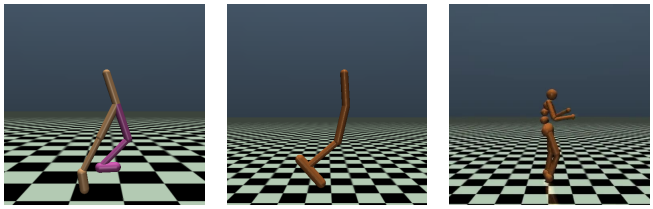

Figure 2: Visualization of Walker2d-v2 (left), Hopper-v2 (middle) and Humanoid-v2 (right).

4.1 True Reward Function

In a first experiment, we compare Composite TD3, TD3(Δ) and conventional TD3 with both the optimized default learning rate and the highest learning rate used in Composite TD3 (TD3 HL) on the true reward for the Walker2d-v2 environment in Figure 3a over 8 training runs. Composite TD3 and TD3(Δ) yield a better and more stable performance than TD3 with either learning rate, with Composite TD3 being the best performing of all approaches. The differences between conventional TD3 and Composite TD3 are significant, as shown in Table E.1 in the appendix. TD3 is not able to gain performance with higher

learning rate and even degenerates. Composite TD3 and TD3(Δ) show less variance.

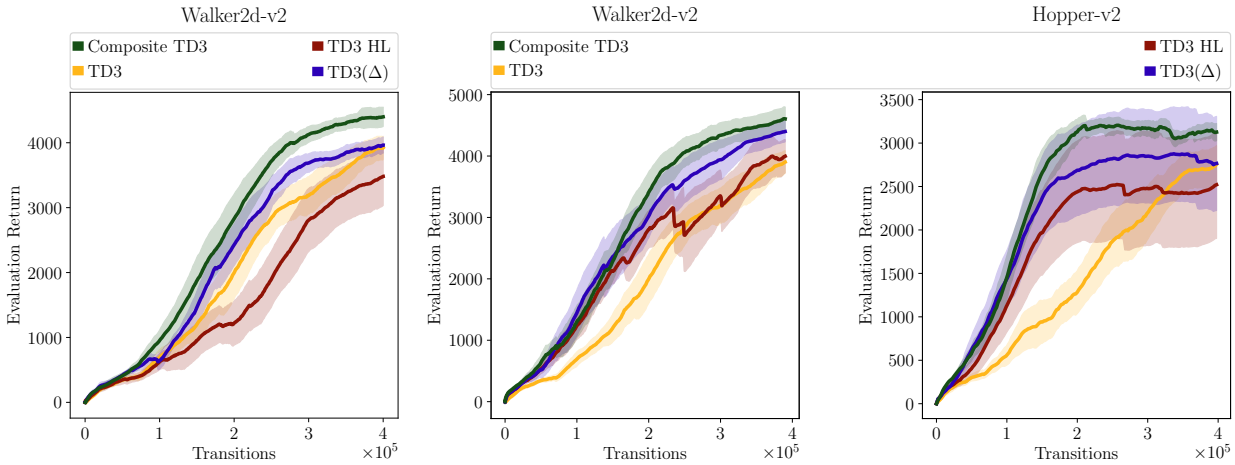

(a) (b)

Figure 3: (a) Mean performance and half a SD over 8 training runs for the Walker2d-v2 environment with the default reward. (b) Results over 8 training runs of Composite Q-learning on the vanilla reward function and multiple update steps per collected sample for the Walker2d-v2 and Hopper-v2 environment.

In a further experiment using the true reward, we investigate the potential increase in data-efficiency when applying multiple gradient steps per collected sample. Results over 8 training runs can be seen in Figure 3b, with corresponding significance tests provided in Table E.1 in the appendix. While there seems to be a limit in benefit for TD3 w.r.t. multiple gradient steps, Composite TD3 and TD3(Δ) yield a faster learning speed. In addition, Composite Q-learning has no increase in variance opposed to all other approaches. The high learning rate in combination with multiple gradient steps is harmful w.r.t. learning stability. Results on different truncation horizons n in the Walker2d-v2 environment are depicted in Figure 4. It can be seen that there is a trade-off between complexity of truncated value-estimation and the faster composition of the value by the Shifted Q-functions.

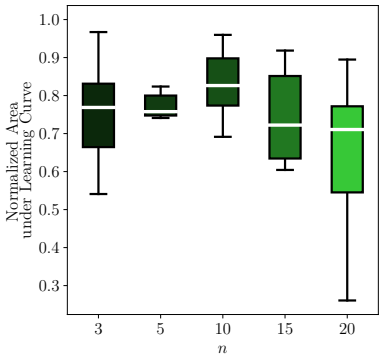

Figure 4: Normalized area under the learning curve for Composite TD3 in the Walker2d-v2 environment with different truncation horizons n. The plot shows median and interquartile ranges over 8 training runs, each representing mean evaluation performance over 100 initial states.

4.2 Noisy Reward Function

We evaluate Composite TD3 under a noisy reward function and compare to TD3, TD3 with high learning rate and TD3(Δ). The immediate reward is replaced by a uniform sample $u \sim \mathcal{U}[-1, 1]$ with 40% chance,

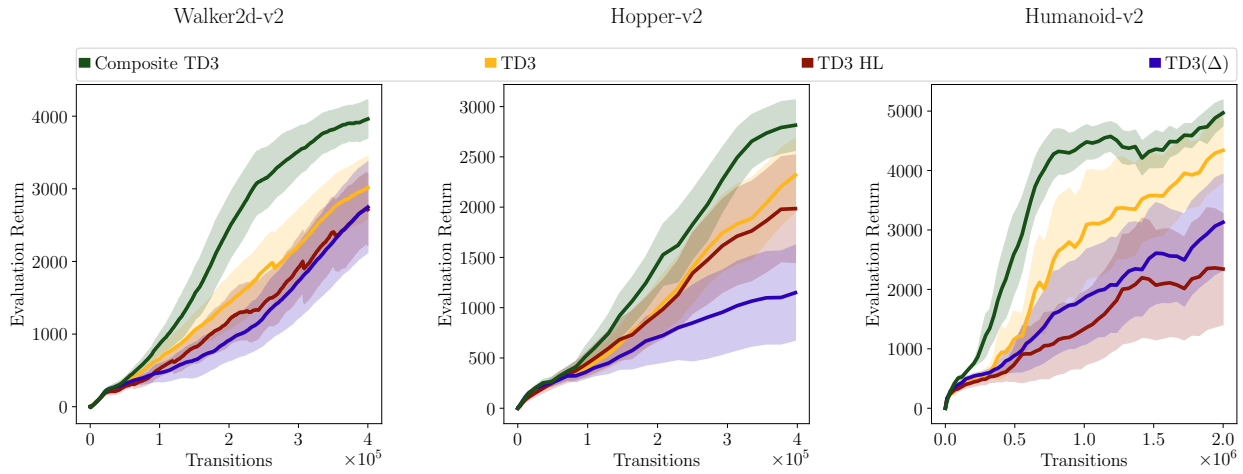

Figure 5: Mean performance and half a SD over 8 training runs for (left) Walker2d-v2, (middle) Hopper-v2 and (right) Humanoid-v2 with uniform noise on the reward function as in (Romoff et al., 2019).

corresponding to the strongest noise level described in (Romoff et al., 2019). In order to account for the high variance, we provide mean and standard deviation (SD) over 8 runs. Results can be seen in Figure 5, corresponding significance tests are provided in Table E.2 in the appendix. Composite TD3 proves to be very robust, even for the very complex Humanoid-v2 environment. All other approaches suffer from slower learning speed and high variance. This holds especially for TD3 with high learning rate and TD3(Δ). We believe this to be caused by overfitting to the noisy reward function due to the high learning rate in TD3 HL and due to the low gamma of the first value-functions in TD3(Δ). Since all other predictions only add to the prediction of the preceding head, there is nothing to prevent the overestimation bias from being propagated to the other outputs of higher discount value. In Composite Q-learning however, Shifted and Truncated Q-functions estimate distinct parts of the temporal chain. This is also highlighted in Figure 6, where the TD-errors of Shifted and Truncated Q-functions can be seen along with learning curves of Humanoid-v2. Whilst in the default setting with vanilla reward the Truncated Q-functions are converging much faster than the Shifted Q-function due to the simpler problem induced by the smaller horizon, the opposite holds in case of the noisy reward. In these experiments, the Truncated Q-functions are not capable of an accurate prediction within the given time frame, yet the Shifted Q-functions can construct an accurate chain given those inaccurate predictions reliably leading to a well-performing policy. This backs our hypothesis that Shifted Q-functions can benefit from higher learning rates also in noisy reward settings whereas Truncated Q-functions have to account for variance in the reward as well, which adds to the complexity of the problem significantly. This translates to faster learning, as underlined by the results in Table 1.

Table 1: Mean normalized area under the learning curve and SD over 8 training runs of Composite TD3 in the noisy reward experiments.

Method	Walker2d-v2	Hopper-v2	Humanoid-v2
TD3	$68\% \pm 22\%$	$76\% \pm 28\%$	$68\% \pm 30\%$
TD3 (HL)	$56\% \pm 18\%$	$72\% \pm 37\%$	$38\% \pm 29\%$
TD3(Δ)	$52\% \pm 23\%$	$49\% \pm 31\%$	$56\% \pm 26\%$
Composite TD3	$\mathbf{100\% \pm 20\%}$	$\mathbf{100\% \pm 25\%}$	$\mathbf{100\% \pm 16\%}$

Table 2 shows the mean maximum return achieved by Composite TD3, TD3 with default and high learning rate and TD3(Δ). Composite TD3 reaches significantly higher returns with lowest variance compared to vanilla TD3 when applied to a noisy reward function, especially for the most complex environment Humanoid-v2.

Table 2: Mean maximum return and SD over 8 training runs for the noisy reward experiments.

Method	Walker2d-v2	Hopper-v2	Humanoid-v2
TD3	3063 ± 813	2386 ± 729	4453 ± 1070
TD3 (HL)	2950 ± 866	2124 ± 1054	2506 ± 2004
TD3(Δ)	2772 ± 1245	1242 ± 954	3251 ± 1687
Composite TD3	$\mathbf{4041 \pm 476}$	$\mathbf{2931 \pm 457}$	$\mathbf{5019 \pm 404}$

Our experimental results show that Composite Q-learning offers a significant improvement over traditional Q-learning methods and a great potential for real-world applications such as learning directly on real robots, where the extraction of the immediate reward signal can be noisy due to occlusions, complex training setups, sensor and actuator noise, or fitted reward functions.

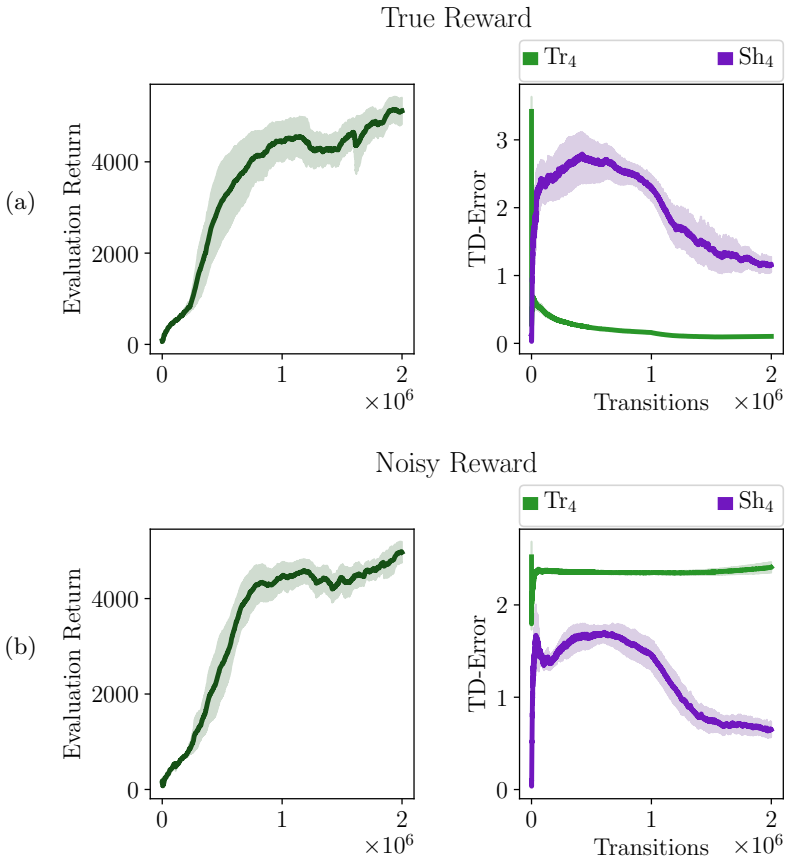

Figure 6: Performance and TD-errors on Humanoid-v2 of Truncated and Shifted Q-functions at $n = 4$ w.r.t. the (a) vanilla and (b) noisy reward. Please note that *TD-error* here means the deviation from the associated target.

5 Conclusion

We introduced Composite Q-learning, an off-policy reinforcement learning method that divides learning of the full long-term value into a series of well-defined shorter prediction horizon estimates. It combines Truncated Q-functions acting on a short horizon with Shifted Q-functions for the remainder of the rollout. As a baseline, we further introduced and evaluated TD3(Δ), an off-policy variant of TD(Δ). We showed on three simulated robot learning tasks that compositional Q-learning methods can be of advantage w.r.t.

data-efficiency compared to vanilla Q-learning methods and that Composite TD3 outperforms vanilla TD3 by 24% - 32% in terms of area under the learning curve. In addition, Composite Q-learning proved to be very robust to noisy reward signals which is very important for real-world applications where the immediate reward may depend on a stochastic next state or where the reward function is estimated from data.

Going forward, using ensemble uncertainty estimates based on the variance of all predictions from the Composite Q-function could be of benefit in update calculation, transition sampling and exploration. We further believe our method to be a better fit for non-stationary reward functions than traditional Q-learning methods due to the flexibility provided by the divided long-term return. Representing the farsighted return after n steps of a policy rollout in the future, Shifted Q-functions could serve as an implicit dynamics model to further build the bridge between model-based and model-free methods.

References

Oron Anschel, Nir Baram, and Nahum Shimkin. Averaged-dqn: Variance reduction and stabilization for deep reinforcement learning. In *ICML*, volume 70 of *Proceedings of Machine Learning Research*, pp. 176–185. PMLR, 2017.

Kristopher De Asis, Alan Chan, Silviu Pitis, Richard S. Sutton, and Daniel Graves. Fixed-horizon temporal difference methods for stable reinforcement learning. In *The Thirty-Fourth AAAI Conference on Artificial Intelligence, AAAI 2020, The Thirty-Second Innovative Applications of Artificial Intelligence Conference, IAAI 2020, The Tenth AAAI Symposium on Educational Advances in Artificial Intelligence, EAAI 2020, New York, NY, USA, February 7-12, 2020*, pp. 3741–3748. AAAI Press, 2020.

Anonymous Authors. Adversarial skill networks: Unsupervised robot skill learning from video. In *ICRA*, pp. 4188–4194. IEEE, 2020a.

Anonymous Authors. Dynamically balanced value estimates for actor-critic methods, 2020b.

Philip J. Ball and Stephen J. Roberts. Offcon^3: What is state of the art anyway? *CoRR*, abs/2101.11331, 2021.

Greg Brockman, Vicki Cheung, Ludwig Pettersson, Jonas Schneider, John Schulman, Jie Tang, and Wojciech Zaremba. Openai gym. *CoRR*, abs/1606.01540, 2016.

Justin Fu, Avi Singh, Dibya Ghosh, Larry Yang, and Sergey Levine. Variational inverse control with events: A general framework for data-driven reward definition. In *Advances in Neural Information Processing Systems*, volume 31. Curran Associates, Inc., 2018.

Scott Fujimoto, Herke van Hoof, and David Meger. Addressing function approximation error in actor-critic methods. In *Proceedings of the 35th International Conference on Machine Learning, ICML*, volume 80 of *Proceedings of Machine Learning Research*, pp. 1582–1591. PMLR, 2018.

Tuomas Haarnoja, Aurick Zhou, Pieter Abbeel, and Sergey Levine. Soft actor-critic: Off-policy maximum entropy deep reinforcement learning with a stochastic actor. In *ICML*, volume 80 of *Proceedings of Machine Learning Research*, pp. 1856–1865. PMLR, 2018.

Tuomas Haarnoja, Sehoon Ha, Aurick Zhou, Jie Tan, George Tucker, and Sergey Levine. Learning to walk via deep reinforcement learning. In *Proceedings of Robotics: Science and Systems*, 2019.

Diederik P. Kingma and Jimmy Ba. Adam: A method for stochastic optimization. In *3rd International Conference on Learning Representations, ICLR 2015, San Diego, CA, USA, May 7-9, 2015, Conference Track Proceedings*, 2015.

Timothy P. Lillicrap, Jonathan J. Hunt, Alexander Pritzel, Nicolas Heess, Tom Erez, Yuval Tassa, David Silver, and Daan Wierstra. Continuous control with deep reinforcement learning. In *4th International Conference on Learning Representations, ICLR*, 2016.

Volodymyr Mnih, Koray Kavukcuoglu, David Silver, Andrei A. Rusu, Joel Veness, Marc G. Bellemare, Alex Graves, Martin A. Riedmiller, Andreas Fidjeland, Georg Ostrovski, Stig Petersen, Charles Beattie, Amir Sadik, Ioannis Antonoglou, Helen King, Dharshan Kumaran, Daan Wierstra, Shane Legg, and Demis Hassabis. Human-level control through deep reinforcement learning. *Nature*, 518(7540):529–533, 2015.

Tianwei Ni, Harshit S. Sikchi, Yufei Wang, Tejus Gupta, Lisa Lee, and Benjamin Eysenbach. f-irl: Inverse reinforcement learning via state marginal matching. *CoRR*, abs/2011.04709, 2020.

Martin Riedmiller, Roland Hafner, Thomas Lampe, Michael Neunert, Jonas Degrave, Tom van de Wiele, Vlad Mnih, Nicolas Heess, and Jost Tobias Springenberg. Learning by playing solving sparse reward tasks from scratch. In *Proceedings of the 35th International Conference on Machine Learning*, volume 80 of *Proceedings of Machine Learning Research*, pp. 4344–4353. PMLR, 10–15 Jul 2018.

Joshua Romoff, Peter Henderson, Alexandre Piché, Vincent François-Lavet, and Joelle Pineau. Reward estimation for variance reduction in deep reinforcement learning. In *2nd Annual Conference on Robot Learning, CoRL 2018, Zürich, Switzerland, 29-31 October 2018, Proceedings*, volume 87 of *Proceedings of Machine Learning Research*, pp. 674–699. PMLR, 2018.

Joshua Romoff, Peter Henderson, Ahmed Touati, Yann Ollivier, Emma Brunskill, and Joelle Pineau. Separating value functions across time-scales. *CoRR*, abs/1902.01883, 2019.

David Silver, Guy Lever, Nicolas Heess, Thomas Degris, Daan Wierstra, and Martin A. Riedmiller. Deterministic policy gradient algorithms. In *Proceedings of the 31th International Conference on Machine Learning, ICML*, volume 32 of *JMLR Workshop and Conference Proceedings*, pp. 387–395, 2014.

David Silver, Thomas Hubert, Julian Schrittwieser, Ioannis Antonoglou, Matthew Lai, Arthur Guez, Marc Lanctot, Laurent Sifre, Dharshan Kumaran, Thore Graepel, et al. A general reinforcement learning algorithm that masters chess, shogi, and go through self-play. *Science*, 362(6419):1140–1144, 2018.

Emanuel Todorov, Tom Erez, and Yuval Tassa. Mujoco: A physics engine for model-based control. In *IEEE/RSJ International Conference on Intelligent Robots and Systems, IROS*, pp. 5026–5033. IEEE, 2012.

Hado van Hasselt, Arthur Guez, and David Silver. Deep reinforcement learning with double q-learning. In *Proceedings of the 30th AAAI Conference on Artificial Intelligence*, pp. 2094–2100. AAAI Press, 2016.

Christopher JCH Watkins and Peter Dayan. Q-learning. *Machine learning*, 8(3-4):279–292, 1992.

A Theory of Composite Q-learning

First, we provide a theoretical foundation for Composite Q-learning. We show that the Composite Q-target is a complete representation of the full return by analyzing the Truncated Q-target in Theorem A.1, the Shifted Q-target in Theorem A.2 and the full Composite Q-target in Theorem A.3.

Theorem A.1. *Let $Q_1^\pi(s_t, a_t) = r_t$ be the one-step Truncated Q-function and $Q_{i>1}^\pi(s_t, a_t) = r_t + \gamma \mathbf{E}_{t,\pi,\mathcal{M}}[Q_{i-1}^\pi(s_{t+1}, a_{t+1})]$ the i-step Truncated Q-function. Then $Q_i^\pi(s_t, a_t)$ represents the truncated return $Q_i^\pi(s_t, a_t) = \mathbf{E}_{t,\pi,\mathcal{M}}[\sum_{j=t}^{t+i-1} \gamma^{j-t} r_j]$.*

Proof. Proof by induction. $Q_1^\pi(s_t, a_t) = r_t$ by definition. The theorem follows from induction step:

$$
\begin{aligned}
Q_i^\pi(s_t, a_t) &= r_t + \gamma \mathbf{E}_{\pi,\mathcal{M}} \left[Q_{i-1}^\pi(s_{t+1}, a_{t+1}) \right] \\
&= r_t + \gamma \mathbf{E}_{\pi,\mathcal{M}} \left[\sum_{j=(t+1)}^{(t+1)+(i-1)-1} \gamma^{j-(t+1)} r_j \right] \\
&= r_t + \gamma \mathbf{E}_{\pi,\mathcal{M}} \left[\sum_{j=(t+1)}^{t+i-1} \gamma^{j-(t+1)} r_j \right] \\
&= r_t + \mathbf{E}_{\pi,\mathcal{M}} \left[\sum_{j=(t+1)}^{t+i-1} \gamma^{j-t} r_j \right] \\
&= \mathbf{E}_{\pi,\mathcal{M}} \left[\sum_{j=t}^{t+i-1} \gamma^{j-t} r_j \right].
\end{aligned}
$$

□

Theorem A.2. *Let $Q_{1:\infty}^\pi(s_t, a_t) = \mathbf{E}_{t,\pi,\mathcal{M}}[\gamma Q^\pi(s_{t+1}, a_{t+1})]$ be the one-step Shifted Q-function and $Q_{i>1:\infty}^\pi(s_t, a_t) = \mathbf{E}_{t,\pi,\mathcal{M}}[\gamma Q_{i-1:\infty}^\pi(s_{t+1}, a_{t+1})]$ the i-step Shifted Q-function. Then $Q_{i:\infty}^\pi(s_t, a_t)$ represents the shifted return $Q_{i:\infty}^\pi(s_t, a_t) = \mathbf{E}_{t,\pi,\mathcal{M}}[\gamma^i Q^\pi(s_{t+i}, a_{t+i})]$.*

Proof. Proof by induction. $Q_{1:\infty}^\pi(s_t, a_t) = \mathbf{E}_{\pi,\mathcal{M}}[\gamma Q^\pi(s_{t+1}, a_{t+1})]$ by definition. The theorem follows from induction step:

$$
\begin{aligned}
Q_{i:\infty}^\pi(s_t, a_t) &= \mathbf{E}_{\pi,\mathcal{M}} \left[\gamma Q_{i-1:\infty}^\pi(s_{t+1}, a_{t+1}) \right] \\
&= \mathbf{E}_{\pi,\mathcal{M}} \left[\gamma(\gamma^{i-1} Q^\pi(s_{t+1+i-1}, a_{t+1+i-1})) \right] \\
&= \mathbf{E}_{\pi,\mathcal{M}} \left[\gamma(\gamma^{i-1} Q^\pi(s_{t+i}, a_{t+i})) \right] \\
&= \mathbf{E}_{\pi,\mathcal{M}} \left[\gamma^i Q^\pi(s_{t+i}, a_{t+i}) \right].
\end{aligned}
$$

□

Theorem A.3. *Let $Q_n^\pi(s_t, a_t) = \mathbf{E}_{t,\pi,\mathcal{M}}[\sum_{j=t}^{t+n-1} \gamma^{j-t} r_j]$ be the truncated return and $Q_{n:\infty}^\pi(s_t, a_t) = \mathbf{E}_{t,\pi,\mathcal{M}}[\gamma^n Q(s_{t+n}, a_{t+n})]$ the shifted return. Then $Q^\pi(s_t, a_t) = Q_n^\pi(s_t, a_t) + Q_{n:\infty}^\pi(s_t, a_t)$ represents the full return, i.e. $Q^\pi(s_t, a_t) = \mathbf{E}_{t,\pi,\mathcal{M}}[\sum_{j=t}^{\infty} \gamma^{j-t} r_j]$.*

Proof.

$$
\begin{aligned}
Q^\pi(s_t, a_t) &= Q^\pi_n(s_t, a_t) + Q^\pi_{n:\infty}(s_t, a_t) \\
&= \mathbf{E}_{\pi,\mathcal{M}}\left[\sum_{j=t}^{t+n-1} \gamma^{j-t} r_j + \gamma^n Q^\pi(s_{t+n}, a_{t+n})\right] \\
&= \mathbf{E}_{\pi,\mathcal{M}}\left[\sum_{j=t}^{t+n-1} \gamma^{j-t} r_j + \gamma^n \left(Q^\pi_n(s_{t+n}, a_{t+n}) + Q^\pi_{n:\infty}(s_{t+n}, a_{t+n})\right)\right] \\
&= \mathbf{E}_{\pi,\mathcal{M}}\left[\sum_{j=t}^{t+n-1} \gamma^{j-t} r_j + \gamma^n \left(\sum_{j=t+n}^{t+2n-1} \gamma^{j-t-n} r_j + \gamma^n Q^\pi(s_{t+2n}, a_{t+2n})\right)\right] \\
&= \mathbf{E}_{\pi,\mathcal{M}}\left[\sum_{j=t}^{t+n-1} \gamma^{j-t} r_j + \sum_{j=t+n}^{t+2n-1} \gamma^{j-t} r_j + \gamma^{2n} Q^\pi(s_{t+2n}, a_{t+2n})\right] \\
&= \mathbf{E}_{\pi,\mathcal{M}}\left[\sum_{j=t}^{t+2n-1} \gamma^{j-t} r_j + \gamma^{2n} Q^\pi(s_{t+2n}, a_{t+2n})\right].
\end{aligned}
$$

By induction, it follows $Q^\pi(s_t, a_t) = \mathbf{E}_{\pi,\mathcal{M}}[\sum_{j=t}^{\infty} \gamma^{j-t} r_j]$. □

B Tabular Composite Q-learning

In Algorithm B.1 you find a description of tabular Composite Q-learning as used in our experiments in Appendix C.

Algorithm B.1: Tabular Composite Q-learning

initialize Truncated Q-functions Q_i
initialize Shifted Q-functions $Q_{i:\infty}$
initialize Q-function Q
for *episode* $= 1..E$ **do**
  get initial state s_1
  for $t = 1..T$ **do**
    apply ϵ-greedy action a_t
    observe s_{t+1} and r_t
    update Truncated Q-functions by:
      $Q_1(s_t, a_t) \leftarrow (1 - \alpha_{\text{Tr}})Q_1(s_t, a_t) + \alpha_{\text{Tr}} r_t$
      $Q_{i>1}(s_t, a_t) \leftarrow (1 - \alpha_{\text{Tr}})Q_i(s_t, a_t) + \alpha_{\text{Tr}}(r_t + \gamma Q_{i-1}(s_{t+1}, \arg\max_a Q(s_{t+1}, a)))$
    update Shifted Q-functions by:
      $Q_{1:\infty}(s_t, a_t) \leftarrow (1 - \alpha_{\text{Sh}})Q_{1:\infty}(s_t, a_t) + \alpha_{\text{Sh}}(\gamma \max_a Q(s_{t+1}, a))$
      $Q_{(i>1):\infty}(s_t, a_t) \leftarrow (1 - \alpha_{\text{Sh}})Q_{i:\infty}(s_t, a_t) + \alpha_{\text{Sh}}(\gamma Q_{(i-1):\infty}(s_{t+1}, \arg\max_a Q(s_{t+1}, a)))$
    update Q-function by:
      $Q(s_t, a_t) \leftarrow (1 - \alpha_Q)Q(s_t, a_t) + \alpha_Q(r_t + \gamma(Q_n(s_{t+1}, \arg\max_a Q(s_{t+1}, a))$
      $+ Q_{n:\infty}(s_{t+1}, \arg\max_a Q(s_{t+1}, a))))$

C Evaluation of Tabular Composite Q-learning

C.1 Deterministic Chain

We evaluate the effect of composing the long-term return of multiple short-term predictions in the tabular setting. We apply Composite Q-learning in the tabular case to the MDP of horizon K given in Figure C.1a.

We compare Composite Q-learning to vanilla Q-learning, as well as multi-step Q-learning based on subtrajectories of the exploratory policy and imaginary rollouts of the target-policy with the true model of the MDP as a hypothetical lower bound on the required updates.

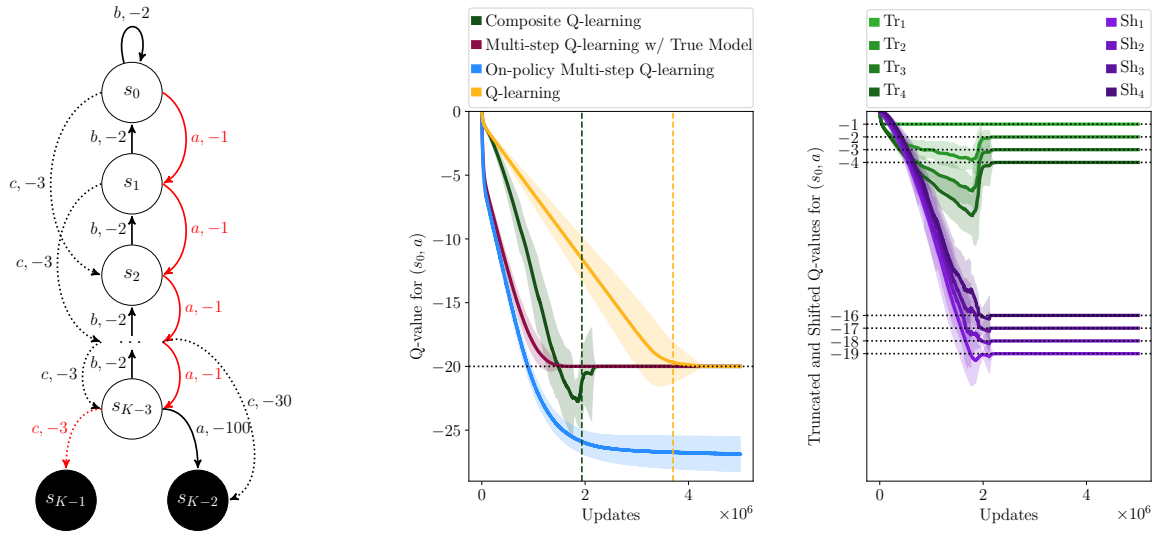

(a) (b)

Figure C.1: (a) In this deterministic-chain MDP of horizon K, the agent ought to arrive at terminal state s_{K-1} using actions $\{a, b, c\}$. The initial state is s_0 and the optimal policy is given in red. (b) Mean results and two standard deviations over 10 runs on the MDP with a horizon of $K = 20$. The left plot depicts the value of s_0 and action a as estimated by the different approaches over time. Dashed lines indicate convergence to the optimal policy. The predicted Truncated Q-values for state s_0 and action a with horizons 1 to 4, denoted by $\mathrm{Tr}_1, \dots, \mathrm{Tr}_4$, and predicted Shifted Q-values for state s_0 and action a, denoted by $\mathrm{Sh}_1, \dots, \mathrm{Sh}_4$, are to the right. Dotted lines indicate the true optimal respective Q-values.

Results for $K = 20$ are depicted in Figure C.1b, where mean performances of the approaches are shown on the left and the intermediate predictions of Composite Q-learning on the right. All approaches update the Q-function with a learning rate of 10^{-3} on the same fixed batch of 10^3 episodes with a percentage of 10% non-optimal transitions. We set rollout length $n = 4$ for all respective approaches. Please note that this value can be set arbitrarily, however in order to be beneficial it should be set to a value smaller than the temporal horizon of the task. In this example, a rollout length of 4 corresponds to the integer square root of the horizon of the MDP, meaning that Truncated and Shifted Q-functions have a similar temporal horizon due to the partitioning of the long-term value. An evaluation of the performance for different rollout lengths n is shown in Figure C.2.

Table C.1: Comparison of convergence speed between Tabular Q-learning and Tabular Composite Q-learning for exemplary runs on the MDP given in Figure C.1a with $n = 4$.

Horizon K	10	20	50	100
Speed up over Q-learning	11%	44%	57%	66%

For the experiments in Figure C.1b, we update the Shifted Q-function with a learning rate of 10^{-2} and the Truncated Q-functions with a learning rate of 10^{-3}. Composite Q-learning converges much faster to the true action-value than vanilla Q-learning and is close to the multi-step approach based on model rollouts (hypothetical lower bound). The erroneous updates of on-policy multi-step Q-learning lead to convergence

to a wrong action-value which is underlining the importance of truly off-policy learning.

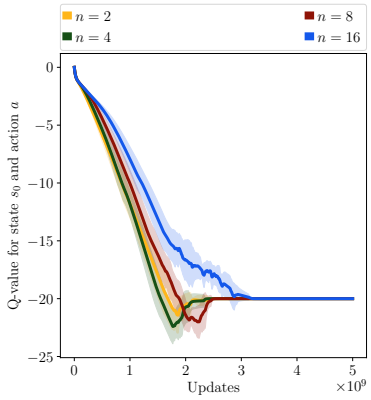

Figure C.2: Performance of Composite Q-learning applied to the MDP in Figure C.1a with different rollout lengths n.

Composite Q-learning estimates the short-term rollouts off-policy by design and shifts the long-term value in time so as to have a consistent temporal chaining. All intermediate predictions therefore converge to the true intermediate action-values, which is shown on the right side of Figure C.1b. The difference in convergence speed between Q-learning and Composite Q-learning grows with increasing horizon, as shown in Table C.1 for the described hyperparameter setting.

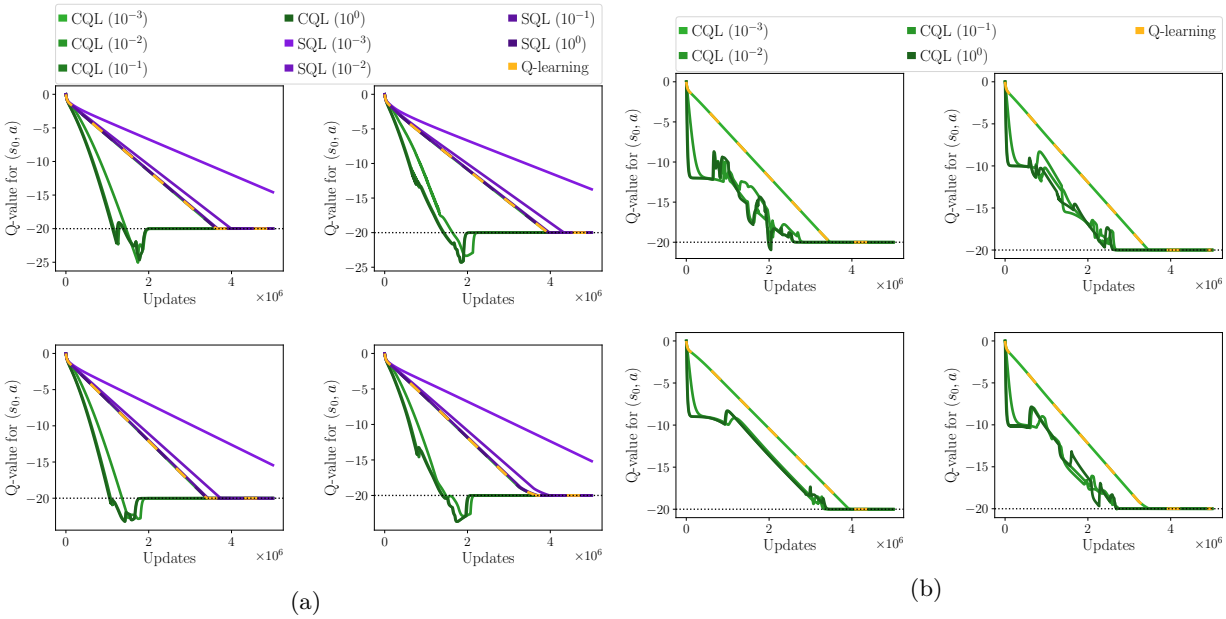

Figure C.3: Results of 4 individual runs on the deterministic chain MDP with a horizon of $K = 20$ for Composite and Shifted Q-learning, (a) with different learning rates for the Shifted Q-function and (b) with different learning rates for the Truncated Q-function (denoted by the numbers in parentheses). The learning rates for the full Q-function and for the (a) Truncated Q-functions and the (b) Shifted Q-functions are set to 10^{-3} in all experiments.

Next, we present an evaluation of different learning rates for the Shifted Q-functions, depicted in Figure C.3a. Here we compare Composite Q-learning (CQL) and vanilla Q-learning to Shifted Q-learning (SQL), which corresponds to Q-learning with a one-step shifted target (replacing the bootstrap of the future return with

an evaluation of a one-step Shifted Q-function and without approximate n-step returns from a Truncated Q-function). The results show that shifting the value in time alone is slowing down convergence. Precisely, Shifted Q-learning with a learning rate of 1.0 is equivalent to vanilla Q-learning; the same holds for Composite Q-learning with a learning rate of 10^{-3} for the Shifted Q-function.

Please note that although the learning rate of Q-learning could be set to a higher value for this very MDP, this example shows the benefit of Composite Q-learning even though higher learning rates for Shifted Q-functions alone do not bring any speedup in convergence. Only the combination of Shifted Q-functions and Truncated Q-functions lead to an increase of convergence speed, even in the case when Truncated and full Q-function are estimated with the same (slow) learning rate of 10^{-3}. The results underline that the higher learning rates for the Shifted Q-functions only have a beneficial effect in combination with truncated predictions.

The counterpart with different learning rates for the Truncated Q-functions, keeping the learning rates for the full Q-estimate and Shifted Q-functions fixed, can be seen in Figure C.3b. While there is improvement in convergence using a larger learning rate for the Truncated Q-functions, the results show higher variance and less benefit than the Shifted Q-functions in Figure C.3a.

C.2 Stochastic Chain

We further investigate the effect of stochastic immediate rewards on Composite Q-learning on the chain MDP shown in Figure C.4. All actions lead further into the chain, however they yield different expected rewards. Action a has an expected reward of -0.8, corresponding to an immediate reward of -1 with 80% chance and 0 with 20%. Action b, on the other hand, has an expected reward of -1.01, however it is $+1$ with 99% chance and -200 with 1%. Composite Q-learning with learning rates of 10^{-2} for the full Q-function, 10^{-1} for the Shifted Q-functions and 10^{-3} for the Truncated Q-functions is compared to Q-learning with the same respective learning rates.

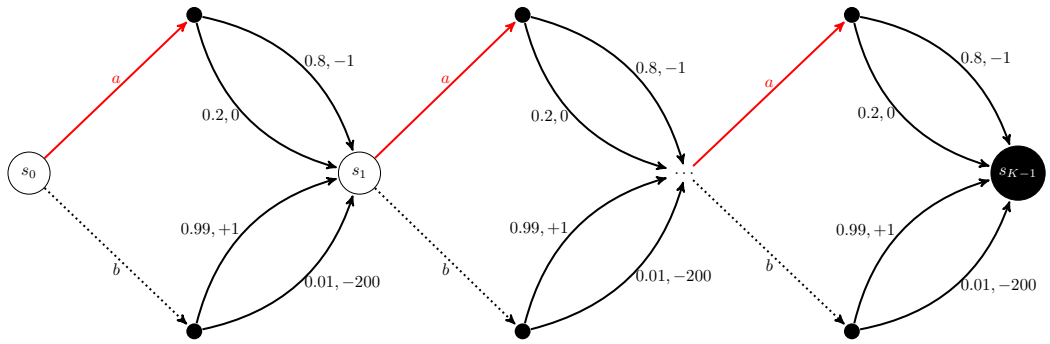

Figure C.4: In this stochastic chain MDP of horizon K, the agent ought to arrive at terminal state s_{K-1} using actions a and b. The initial state is s_0. Transitions are stochastic. The optimal policy is given in red.

Results for different horizons and no discount are depicted in Figure C.5. It can be seen that Q-learning with a high learning rate is converging to a wrong action-value and the deviation becomes more significant the longer the horizon of the task. The same holds for Q-learning with a learning rate of 10^{-2}, however the deviation becomes smaller. Moreover, Q-learning with the same learning rate as the full Q-function in Composite Q-learning is converging much slower for growing horizons, yet the learning rate for the Truncated Q-functions is 10 times smaller than for Q-learning. This emphasizes the mutual interplay of Truncated and Shifted Q-functions. Furthermore, Composite Q-learning is converging to the true optimal action-value. Q-learning with a small learning rate of 10^{-3} is far from achieving a satisfying level of

convergence within the time frame of $2 \cdot 10^7$ updates.

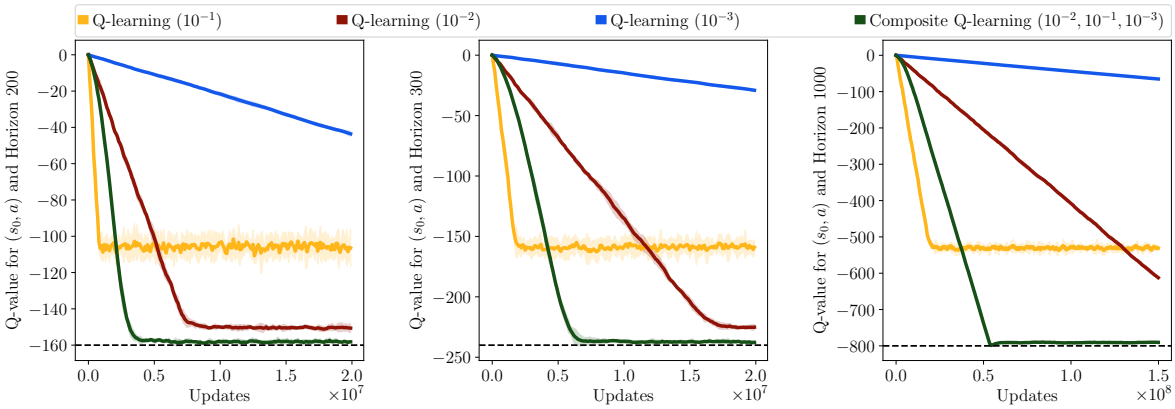

Figure C.5: Results of Composite Q-learning and Q-learning with different learning rates over 5 training runs for horizons (left) 200, (middle) 300 and (right) 1000 and no discount. The true action-value is indicated by the dashed line.

Shifted Q-functions thus allow for higher learning rates which in combination with a more cautious fitting of short-term predictions leads to increased data efficiency while achieving a smaller deviation from the true action-value. Most importantly, the difference in performance between Q-learning and Composite Q-learning (better value estimation w.r.t. to a high learning rate and better convergence properties comparing to a small learning rate) becomes larger for longer horizons. The performance for different rollout lengths are shown in Figure C.6.

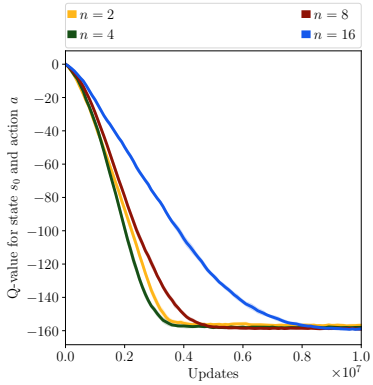

Figure C.6: Performance of Composite Q-learning applied to the MDP in Figure C.4 with different rollout lengths n.

D Hyperparameter Setting and Optimization

D.1 Entropy Regularization

Each pair $Q_i^{\text{Tr}} + Q_i^{\text{Sh}}|_{1 \leq i \leq n}$ is a complete approximation of the true Q-value. Note however, that it is also bootstrapped with the full Q-value. The circular dependency can lead to stability issues, due to the amplification of propagated errors. Additionally, higher learning rates for the Shifted Value-functions, as motivated in Section 3.1.2, may lead to overfitting. In particular, errors in the truncated predictions are propagated quickly by the Shifted Q-functions, especially when trained with a high learning rate. Therefore, it is important to keep the truncated predictions close across the different time steps while also preventing

the Shifted Q-functions from running into suboptimal local minima. As a means to alleviate these issues, we add a regularization based on the entropy of a Gaussian distribution formed by mean $\mu(Q_i^{\mathrm{Tr}} + Q_i^{\mathrm{Sh}}|_{1\leq i\leq n})$ and variance $\sigma^2(Q_i^{\mathrm{Tr}} + Q_i^{\mathrm{Sh}}|_{1\leq i\leq n})$ over all n complete predictions of Q. We can then formalize an incentive of the Truncated Q-functions to stay close between predictions whilst forcing the Shifted Q-functions to keep the distribution as broad as possible. We define the Gaussian distribution $\mathcal{N}_Q$ over all Q-predictions therefore by:

$$\mathcal{N}_Q\left(\mu(Q_i^{\mathrm{Tr}} + Q_i^{\mathrm{Sh}}|_{1\leq i\leq n}), \sigma^2(Q_i^{\mathrm{Tr}} + Q_i^{\mathrm{Sh}}|_{1\leq i\leq n})\right), \tag{12}$$

with corresponding entropy:

$$\mathcal{H}_Q = \frac{1}{2}\log\left(2\pi e\sigma^2(Q_i^{\mathrm{Tr}} + Q_i^{\mathrm{Sh}}|_{1\leq i\leq n})\right). \tag{13}$$

In order to enhance stability of the learning process as a whole while preventing the Shifted Q-functions from overfitting, we not only minimize the mean squared error between targets $y_j^{\mathcal{C}}$ and predictions $Q^{\mathcal{C}}(s_j, a_j|\theta^{\mathcal{C}})$, but apply gradient descent on the entropy for the parameters of Q^{Tr} and gradient ascent on the parameters of Q^{Sh}. More detailed, we define the squared error for some sample j as:

$$\delta_j = \left(y_j^{\mathcal{C}} - Q^{\mathcal{C}}(s_j, a_j|\theta^{\mathcal{C}})\right)^2, \tag{14}$$

and the gradient w.r.t. all parameters of $Q^{\mathcal{C}}$ including the different learning rates as:

$$\xi_j = \alpha_Q\delta_j\nabla_{\theta^Q}Q^{\mathcal{C}}(s_j, a_j|\theta^{\mathcal{C}}) + \alpha_{\mathrm{Tr}}\delta_j\nabla_{\theta^{\mathrm{Tr}}}Q^{\mathcal{C}}(s_j, a_j|\theta^{\mathcal{C}}) + \alpha_{\mathrm{Sh}}\delta_j\nabla_{\theta^{\mathrm{Sh}}}Q^{\mathcal{C}}(s_j, a_j|\theta^{\mathcal{C}}). \tag{15}$$

The regularization then adds to the gradient:

$$\eta_j = \mathcal{H}(s_j, a_j)(\alpha_{\mathrm{Sh}}\beta_{\mathrm{Sh}}\nabla_{\theta^{\mathrm{Sh}}} - \alpha_{\mathrm{Tr}}\beta_{\mathrm{Tr}}\nabla_{\theta^{\mathrm{Tr}}}). \tag{16}$$

Hence, the parameter update in its simplest form becomes:

$$\theta^{\mathcal{C}} \leftarrow \theta^{\mathcal{C}} + \frac{1}{m}\sum_j(\xi_j - \eta_j). \tag{17}$$

However, a more sophisticated optimizer such as Adam (Kingma & Ba, 2015) can be applied analogously.

D.2 Hyperparameter Setting

For all approaches, we use Gaussian noise with $\sigma = 0.15$ for exploration and the optimized learning rate of 10^{-3} for the full Q-function. Target update ($5 \cdot 10^{-3}$) and actor setting (two hidden layers with 400 and 300 neurons and ReLU activation) are set as in (Fujimoto et al., 2018). For Humanoid-v2, we use a slightly changed parameter setting with a learning rate of 10^{-4} for both actor and critic as suggested in (Authors,

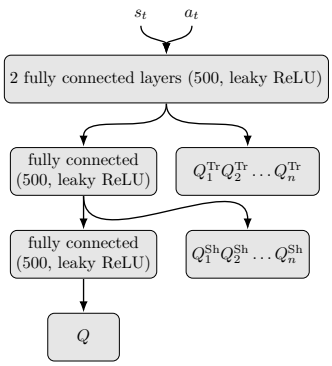

Figure D.1: Optimized architecture of the Composite-Q network used in our experiments.

2020b).

For Composite Q-learning, we calculate the full Q-values, as well as Truncated and Shifted-Q values in one, combined, architecture for improved efficacy. Additionally, we found that it is beneficial to estimate the Truncated and Shifted Q-values in different layers, as depicted in Figure D.1. For all parameters in the layers prior to the full Q-output, we use the parameter setting as described above.

Hyperparameters are optimized for all approaches, including the baselines TD3 and TD3(Δ), for the given subset of MuJoCo tasks via Random Search over 10 training runs with the configuration space shown in Table D.1. Learning rates for the corresponding output layers of the Truncated and Shifted Q-values are optimized individually. We use a learning rate of $6 \cdot 10^{-5}$ for the Truncated Q-functions and $5 \cdot 10^{-3}$ for the Shifted Q-functions. For the noisy experiments, as well as for the experiments with multiple gradient steps per collected sample, we set $n = 4$. For the Walker2d-v2 experiment on the true reward function, we set $n = 10$. In terms of regularization, we set $\beta_{\text{Tr}} = 0.002$ and $\beta_{\text{Sh}} = 0.001$. For Humanoid-v2, we set the optimized learning rates one magnitude lower. When executing multiple gradient steps per collected sample, we keep the learning rate of the Shifted Q-functions at 10^{-3}. We further evaluate TD3 with the same maximum learning rate. We optimize the number of layers and the number of neurons per layer for the critic in Composite Q-learning (4 layers with 500 neurons and leaky ReLU activation) and the architecture for the critic in all other approaches (two layers with 500 neurons and leaky ReLU activation). For an overview of the architecture of the Composite-Q network see Figure D.1. For TD3(Δ), we use the γ-schedule as suggested by Romoff et al. (2019), i.e. $\gamma_1 = 0$ and $\gamma_{i>1} = \frac{\gamma_{i-1}+1}{2}$, with an upper limit of 0.99.

Table D.1: Configuration space of the hyperparameter optimization. For the full Q-function in all approaches, we used the optimized learning rate of 10^{-3} as in (Fujimoto et al., 2018). Hyperparameters denoted by * were optimized individually for all approaches.

Hyperparameter	Values
number of layers*	$\{2, 3, 4\}$
number of neurons*	$\{300, 400, 500\}$
activation*	$\{\text{ReLU}, \text{leaky ReLU}\}$
α_{Tr}	$\{6 \cdot 10^{-6}, 10^{-5}, 6 \cdot 10^{-5}, 10^{-4}, 10^{-3}\}$
α_{Sh}	$\{10^{-3}, 2 \cdot 10^{-3}, 5 \cdot 10^{-3}, 10^{-2}\}$
β_{Tr}	$\{10^{-3}, 2 \cdot 10^{-3}, 4 \cdot 10^{-3}\}$
β_{Sh}	$\{5 \cdot 10^{-4}, 10^{-3}, 2 \cdot 10^{-3}\}$
n	$\{3, 4, 10, 15, 20\}$

D.3 Analysis of Hyperparameters

The influence of the horizon of Truncated and Shifted Q-functions, as well as the respective regularization weights maximizing and minimizing the entropy, is given exemplary for the Walker2d-v2 environment in Figure D.2.

It can be seen that the regularization of the Shifted Q-functions has a higher influence on the performance. If the weight is set too high, the variance increases significantly. The same holds for a too long temporal horizon. The regularization of the Truncated Q-functions has less influence on convergence and variance, however, please note the strong connection of these hyperparameters. Therefore, the best triad setting needs to be found for a given problem and yields an interesting direction for meta-reinforcement learning. Prior experiments with other regularization terms only minimizing the entropy also showed enhanced stability, however, it is important to prevent the Shifted Q-functions from overfitting when applying higher learning rates in the TD3 setting.

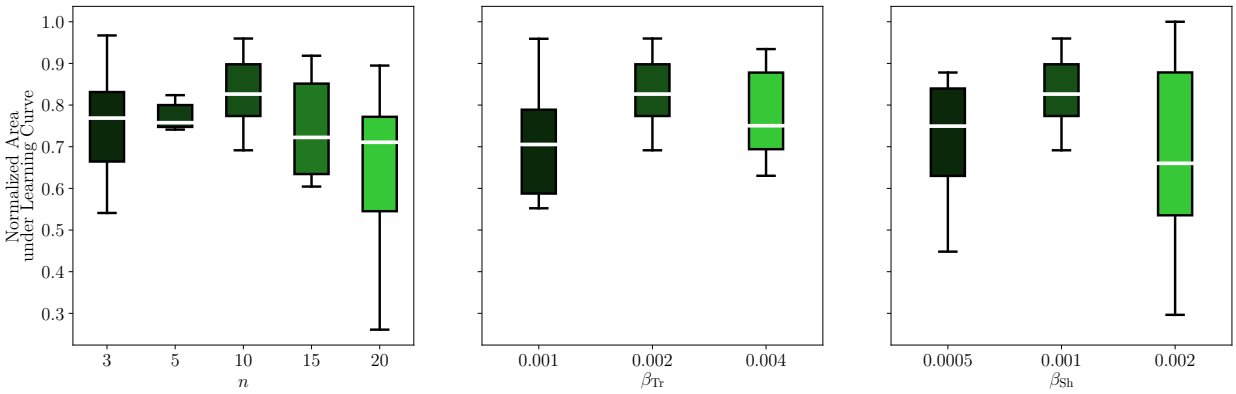

Figure D.2: Normalized area under the learning curve for Composite TD3 in the Walker2d-v2 environment with different truncation horizons n (left) and different regularization weights β^{Tr} (middle) and β^{Sh} (right). The plots show median and interquartile ranges over 8 training runs, each representing mean evaluation performance over 100 initial states.

E Significance Tests

We provide significance tests on the mean area under the learning curve (to account for learning speed and stability) between Composite TD3 and TD3, TD3 (HL) and TD3(Δ). Significance tests for the vanilla reward experiments can be found in Table E.1.

Table E.1: p-values for Welch's t-test on the mean area under the learning curve for 8 different runs of Composite TD3 and all other approaches in the vanilla reward experiments. Subparts (a) and (b) correspond to those in Figure 3.

	TD3	TD3 (HL)	TD3(Δ)
Walker2d-v2 (a)	$8 \cdot 10^{-3}$	$7 \cdot 10^{-4}$	$6 \cdot 10^{-2}$
Walker2d-v2 (b)	$3 \cdot 10^{-4}$	$2 \cdot 10^{-2}$	$5 \cdot 10^{-1}$
Hopper-v2 (b)	$3 \cdot 10^{-5}$	$4 \cdot 10^{-2}$	$5 \cdot 10^{-1}$

Significance tests for the noisy reward experiments can be found in Table E.2.

Table E.2: p-values for Welch's t-test on the mean area under the learning curve for 8 different runs of Composite TD3 and all other approaches in the noisy reward experiments.

	TD3	TD3 (HL)	TD3(Δ)
Walker2d-v2	$4 \cdot 10^{-5}$	$2 \cdot 10^{-8}$	$6 \cdot 10^{-8}$
Hopper-v2	$8 \cdot 10^{-3}$	$8 \cdot 10^{-3}$	$2 \cdot 10^{-6}$
Humanoid-v2	$3 \cdot 10^{-2}$	$4 \cdot 10^{-4}$	$5 \cdot 10^{-6}$